https://doi.org/10.5194/bg-2022-180
Preprint. Discussion started: 4 October 2022

Biogeosciences Discussions

Deep-sea stylasterid $\delta^{18}O$ and $\delta^{13}C$ maps inform sampling scheme for paleotemperature reconstructions

Theresa M. King and Brad E. Rosenheim

College of Marine Science, University of South Florida, St. Petersburg, 33701, USA

Correspondence to: Theresa M. King (theresaking@usf.edu)

Abstract. Deep-sea corals have the potential to provide high resolution paleotemperature records to evaluate oceanographic changes in settings that are vulnerable to current and future warming. The geochemical records preserved in coral skeletal carbonate, however, are limited by their large offsets from isotopic equilibrium with seawater. These "vital effects" are the result of biological influences (kinetic and metabolic) on the calcification of coral skeletons and are well known to drive oxygen and carbon stable isotope ratios ($\delta^{18}O$ and $\delta^{13}C$, respectively) away from an environmental signal. Additionally, vital effects as they pertain to deep-sea branching corals are not well understood, thus hindering the utility of paleoceanographic archives with a vast latitudinal range. Here we describe the likely growth structure of a deep-sea stylasterid coral taxon and demonstrate the optimal sampling location for paleotemperature reconstructions. We sampled two coral specimens over cross sections through their primary growth axes to create skeletal $\delta^{18}O$ and $\delta^{13}C$ maps. Such maps reveal a consistent trend of increasing isotopic values toward the innermost portion of the coral slices; the average center values being ~1‰ closer to seawater equilibrium values than a traditional bulk sample. The difference between the higher center and lower bulk $\delta^{18}O$ values result in temperature difference as much as 5.1° C (±1.8° C) between the sampling methods. These results support a two-step biomineralization consisting of a rapid initial skeletal construction, followed by a slower infilling concentrated towards the center, not yet described for this coral taxon. We anticipate this work to initiate efforts to sample deep-sea branching corals, potentially informing advanced visualization techniques to achieve the most accurate paleotemperature reconstructions.

1 Introduction

Robust paleoceanographic temperature proxies are fundamental to understanding past climate changes and sensitivities. Foundational work developed the theory and application of the oxygen isotope paleothermometer, which was applied to marine biogenic carbonates including foraminiferal tests and shallow water corals (Urey, 1947; McCrea, 1950; Epstein et al., 1953; Emiliani, 1955; Shackleton, 1967; Emiliani et al., 1978). Archives all have limits in geographic distribution despite their ability to lengthen the time domain of our paleoceanographic records. On the Antarctic margin, for instance, foraminifera are not widely present in marine sediment cores. Scleractinian zooxanthellate corals are limited to lower latitudes. Deep-sea corals

https://doi.org/10.5194/bg-2022-180
Preprint. Discussion started: 4 October 2022


Biogeosciences Discussions Open Access EGU

have been used to elucidate ocean history on different time scales (Adkins et al., 1998; Robinson et al., 2005; Robinson and van de Flierdt, 2009; Burke and Robinson, 2012; Chen et al., 2020), but normally the extraction of continuous records from individual colonies has been precluded by the complexity of growth habit and the fidelity of isotope and other records archived in their skeletons (Weber, 1973; Wisshak et al., 2009; Robinson et al., 2014). Corals can incorporate high resolution geochemical records over decades to millennia while remaining fixed to the seafloor, which is especially useful to observe regional and global processes causing seawater stratification to heave and shoal at timescales over which the coral is alive (Andrews et al., 2002; Druffel et al., 1990; Druffel, 1997; Griffin and Druffel, 1989; Risk et al., 2002). Such archives are crucial for paleotemperature reconstructions.

With regard to obtaining high fidelity records of oceanographic change in calcareous skeletons, one must understand that biomineralization of carbonates records both environmental information (signal) and biological effects (noise), also known as "vital effects". Biomineralization can obscure environmental information stored in skeletal records as oxygen and carbon stable isotope ratios ($\delta^{18}O$ and $\delta^{13}C$, respectively). Slow rates of calcification allow for carbon and oxygen isotopes of solid carbonate to approach isotopic equilibrium between skeleton and seawater, a state governed by thermodynamics (McConnaughey, 1989a). Biological calcification, however, includes nonequilibrium fractionation which cannot be interpreted directly as environmental signal (Weber and Woodhead, 1970). Early research on corals demonstrated that isotopic variability can be caused by metabolic fractionation, kinetic fractionation, or a combination of both (McConnaughey, 1989a). The metabolic fractionation is characterized by a change in carbon isotope composition of the dissolved inorganic carbon pool from which the coral calcifies via incorporation of the products of respiration and photosynthesis of algal symbionts or respiration of the coral itself (Swart, 1983; McConnaughey, 1989a). The kinetic fractionation is described as a product of the kinetic isotope effect: discrimination against heavy oxygen and carbon isotopes during hydration and hydroxylation of CO_2 during biomineralization (McConnaughey, 1989b). Rapid calcification results in greater disequilibrium of skeletal $\delta^{18}O$ and $\delta^{13}C$ as the CO_2 does not have sufficient time to equilibrate with ambient seawater before being incorporated into the skeleton (McConnaughey, 1989b). Additional mechanisms for vital effects have been identified more recently, including a biologically mediated pH gradient across coral cell walls (Adkins et al., 2003). Rapid biomineralization drives the pH of internal calcifying fluid toward higher values, increasing the pumping of CO_2, and consequently maximizing fractionation of carbon isotopes (Adkins et al., 2003). Chen et al. (2018) then combined these findings with an additional constraint of kinetic fractionation by the carbonic anhydrase enzyme which catalyzes the hydration and hydroxylation of CO_2 and constructed the most comprehensive model for biomineralization to date.

Because coral specimens from varied ocean depths and latitudes have strong linear relationship between skeletal $\delta^{18}O$ and $\delta^{13}C$ values that trend towards the expected modern equilibrium (Smith et al., 2000; Emiliani et al., 1978; Heikoop et al., 2000; Mikkelsen et al., 2008; McConnaughey, 1989a), vital effects have been employed to discern trends in $\delta^{18}O$ and $\delta^{13}C$ records from deep-sea corals. Isotopic records have largely demonstrated sensitivity to variable rates of calcification. Early work by

https://doi.org/10.5194/bg-2022-180
Preprint. Discussion started: 4 October 2022

(Emiliani et al., 1978) examined the $\delta^{18}O$ and $\delta^{13}C$ recorded by a solitary scleractinian coral and found that both isotopic ratios trended toward higher values from bottom to top of the coral and interpreted this as a slowing growth rate with time, approaching isotopic equilibrium. Additional work on solitary scleractinians by Adkins et al. (2003) employed a microsampling approach for $\delta^{18}O$ and $\delta^{13}C$ that determined the lowest isotopic values occurred at trabecular centers which exhibited the most rapid rates of calcification and were farthest from equilibrium. Bamboo corals sampled across and along their vertical growth axes exhibited low $\delta^{18}O$ and $\delta^{13}C$ values near the innermost portion of the coral and at the distal tips (Hill et al., 2011). Faster calcification in these regions, however, were not supported by calculated growth rates, and there was no consistency among regions of maximum growth rates for a single specimen (Hill et al., 2011). Two studies by Wisshak et al. (2009) and Samperiz et al. (2020) sampled stylasterid corals similar to Hill et al. (2011) and resulted in $\delta^{18}O$ and $\delta^{13}C$ trends with lowest values in the innermost portion of the main coral trunk and at the distal growth tips, supporting rapid growth in those regions. However, Samperiz et al. (2020) noted extensive variability among the $\delta^{18}O$ and $\delta^{13}C$ values within a single growth band (which should represent contemporaneous calcification) as well as variability in isotopic fractionation among different genera and species of stylasterid, supporting heterogeneous calcification. Cumulatively, this results in a lack of clarity regarding colony-scale sampling of deep-sea corals for isolating vital effects to develop robust temperature reconstructions.

Here we establish a link between deep-sea coral growth and isotopic changes, using two deep-dwelling (500 to 1700 m) stylasterid coral specimens, genus *Errina*, to create $\delta^{18}O$ and $\delta^{13}C$ maps over surfaces perpendicular to and along vertical growth axes. Stylasterids are ubiquitous in both latitudinal and depth range, yet remain underrepresented in paleoceanographic reconstructions, due in large part to the lack of understanding of calcification processes (Cairns, 1992). We complement recent work by Samperiz et al. (2020) that has demonstrated the utility of stylasterids to accurately record changes in ocean temperatures by isolating kinetic effects in deep, zooxanthellate-free stylasterids. We compare our skeletal maps to isotopic trends modelled from hypothesized coral growth scenarios and determine that although contradictory to previous research, the isotopic values most representative of environmental signals are recorded in the innermost portion of the coral stems. Ultimately, we prescribe targeted sampling, avoiding the use of bulk drilling methods for the most accurate paleotemperature reconstructions within the *Errina* genus.

2 Methods

2.1 Study location and specimen collection

The Ross Sea is a region of bottom water formation for the worlds' oceans, a characteristic that influences the local oceanography in which the stylasterids live. The region experiences seasonal katabatic winds that create sea ice-forming polynyas, which in turn, create High Salinity Shelf Water through the process of brine rejection (Kurtz and Bromwich, 1985; Picco et al., 2000). The High Salinity Shelf Water flows along the western Ross Sea and out to the shelf edge where it mixes with upwelled modified Circumpolar Deep Water, resulting in a component of dense Antarctic Bottom Water that spills down the continental slope (Gordon et al., 2009; Jacobs et al., 1970; Sandrini et al., 2007).

https://doi.org/10.5194/bg-2022-180
Preprint. Discussion started: 4 October 2022

The stylasterid coral specimens for this study were collected aboard the U.S. Antarctic Program expedition NBP07-01 near Cape Adare in the western Ross Sea. Seamounts on the outer continental shelf were dredged at a water depth ranging 500 m to 1700 m (D05–D09; Fig. 1). The recovered stylasterid corals were predominantly *Errina* spp., most likely *Errina fissurata* based on morphological descriptions (Cairns, 1983a, b, 1991) and scanning electron microscopy (SEM). Specimens were recovered both alive and dead (as evidenced by their pigmentation), some with growth tips intact. For this study, one live-collected and one dead-collected stylasterid were selected (EA-11 and EA-12, respectively), targeting the longest whole specimens ranging from ~8 to 9 cm long (Fig. 2).

2.2 Coral sampling and isotope analysis

The stylasterid specimens were sampled for stable oxygen and carbon isotopic analyses ($\delta^{18}O$ and $\delta^{13}C$, respectively) over cross sections of their major growth stems. A Gryphon diamond band saw was used to slice discs measuring approximately 2–3 mm thick from each specimen's main stems (three from EA-11 and two from EA-12; Fig. 2). Additionally, a longer 8 mm thick section was cut from the lower main stem of EA-11 (Fig. 2). This disc was sliced in half lengthwise with the band saw and sampled along the vertical face. Each coral disc was sonicated in DI water until no remaining loose particles were released, and dried in a 50° C oven for 24 hours. The coral discs were then drilled over their surfaces with a New Wave MicroMill system at grid spacing that varied between 1 and 1.5 mm, based on the diameter of the slice and ampullae in the disc. The MicroMill was configured with a 0.5 mm round carbide bur bit for each hole that plunged to a maximum depth of 1 mm, just far enough to obtain enough carbonate material for analysis (~80–120 µg $CaCO_3$). The carbonate powder from each hole was transferred to vials and the sample hole and stylasterid surface were cleaned with compressed air or nitrogen to remove any residual powder between drilling intervals.

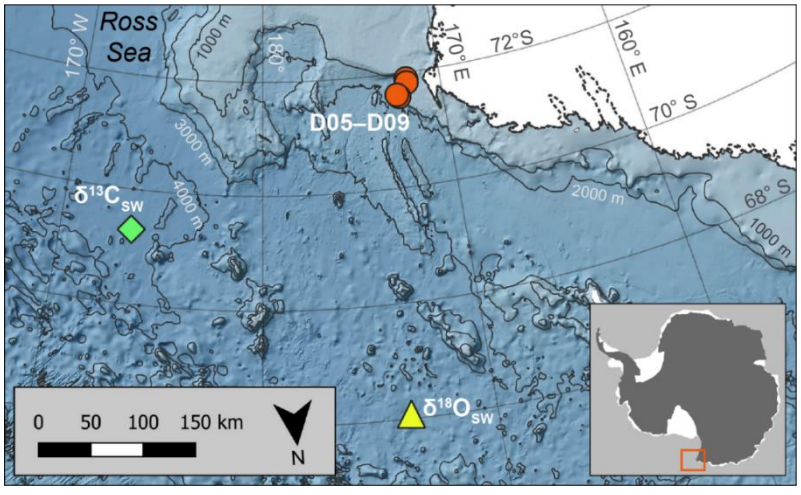

Figure 1: Map of coral collection sites. D05–D09 represent five individual dredge sites from NBP07-01 from which coral samples were collected on the outer western Ross Sea continental shelf. The diamond and triangle mark the stations used to calculate the seawater isotopic ratios ($\delta^{13}C_{sw}$ and $\delta^{18}O_{sw}$; Table S2 in the Supplement). Antarctic landmass and ice sheets are colored white (Gerrish et al., 2022) with the coastline marked by a solid black line, and ice sheet grounding line denoted by a dotted black line (Mouginot et al., 2017). Bathymetric contours are in increments of 500 m (Arndt et al., 2013). Antarctic inset denotes sampling site marked by red box. Map was created using the Quantarctica data set collection within QGIS (Matsuoka et al., 2021).

https://doi.org/10.5194/bg-2022-180
Preprint. Discussion started: 4 October 2022

The sample vials were flushed with helium and acidified with phosphoric acid at 50° C to generate CO_2 that was analyzed at the University of South Florida College of Marine Science using a Thermo Scientific MAT 253 stable isotope ratio mass spectrometer with a Gas Bench II preparatory device. All reported values are in standard delta (δ) notation and reported as per mil (‰). Laboratory reference materials Borba ($\delta^{13}C$: 2.89 ‰, $\delta^{18}O$: -6.15 ‰), TSF-1 ($\delta^{13}C$: 1.95 ‰, $\delta^{18}O$: -2.20 ‰), and Leco ($\delta^{13}C$: -15.44 ‰, $\delta^{18}O$: -20.68 ‰), were used for instrument correction and normalizing to the Pee Dee Belemnite scale (PDB), and an internal Antarctic coral standard was used for quality control. The analytical uncertainty (1σ) of the MAT 253 during this study was ±0.083 ‰ $\delta^{13}C$ and ±0.064 ‰ $\delta^{18}O$.

3 Results

The interior *Errina* skeletons lacked any visible banded growth structure, but were characterized by an outer pink section, and center white section (Fig. 3). The grid spacing of the sampling scheme allowed for microdrilling of several representative samples of both pink and white areas across each coral slice (Table S1 and Fig. S3 in the Supplement). The resulting isotopic records from each slice demonstrate similar overall patterns in that both $\delta^{13}C$ and $\delta^{18}O$ values are higher in the center, white section, and lower in the outer pink section. This trend is observed over each sampling surface of both specimens (Figs. 2 and 3).

Figure 2: Whole coral specimens EA-11 (left) and EA-12 (right). EA-11 was live-collected, and EA-12 was dead. Sample discs are labelled, and the corresponding isotope maps are in Figure 3.

For specimen EA-11, the compilation of $\delta^{18}O$ values ranges from 0.65 ‰ to 2.87 ‰, and the $\delta^{13}C$ values range from -9.56 ‰ to -2.64 ‰, with the minimum values exhibited by EA-11a (nearest the tip) and maximum values by EA-11d (far from the tip). The oxygen isotope ratios of EA-11a range from 0.65 ‰ to 2.48 ‰ and carbon isotope ratios range from -9.56 ‰ to -3.72 ‰. Slice EA-11b has the smallest ranges of $\delta^{18}O$ and $\delta^{13}C$ values for the entire coral specimen at 0.87 ‰ to 2.18 ‰ and -8.61 ‰ to -4.34 ‰, respectively. EA-11c $\delta^{18}O$ values range from 1.08 ‰ to 2.64 ‰ and $\delta^{13}C$ values range from -8.54 ‰ to -2.84 ‰. Lastly, we observed the largest isotope ratio ranges over EA-11d with $\delta^{18}O$ spanning 0.66 ‰ to 2.87 ‰ and $\delta^{13}C$ spanning -8.68 ‰ to -2.64 ‰. For EA-11a through EA-11c, the differences in $\delta^{18}O$ and $\delta^{13}C$ values across each slice are on the order of ~1 ‰ and ~5 ‰, respectively. This variability is unexpected if we assume that each slice/cross section reflects deposition at the same point in time. Therefore, there must be a complex

https://doi.org/10.5194/bg-2022-180
Preprint. Discussion started: 4 October 2022

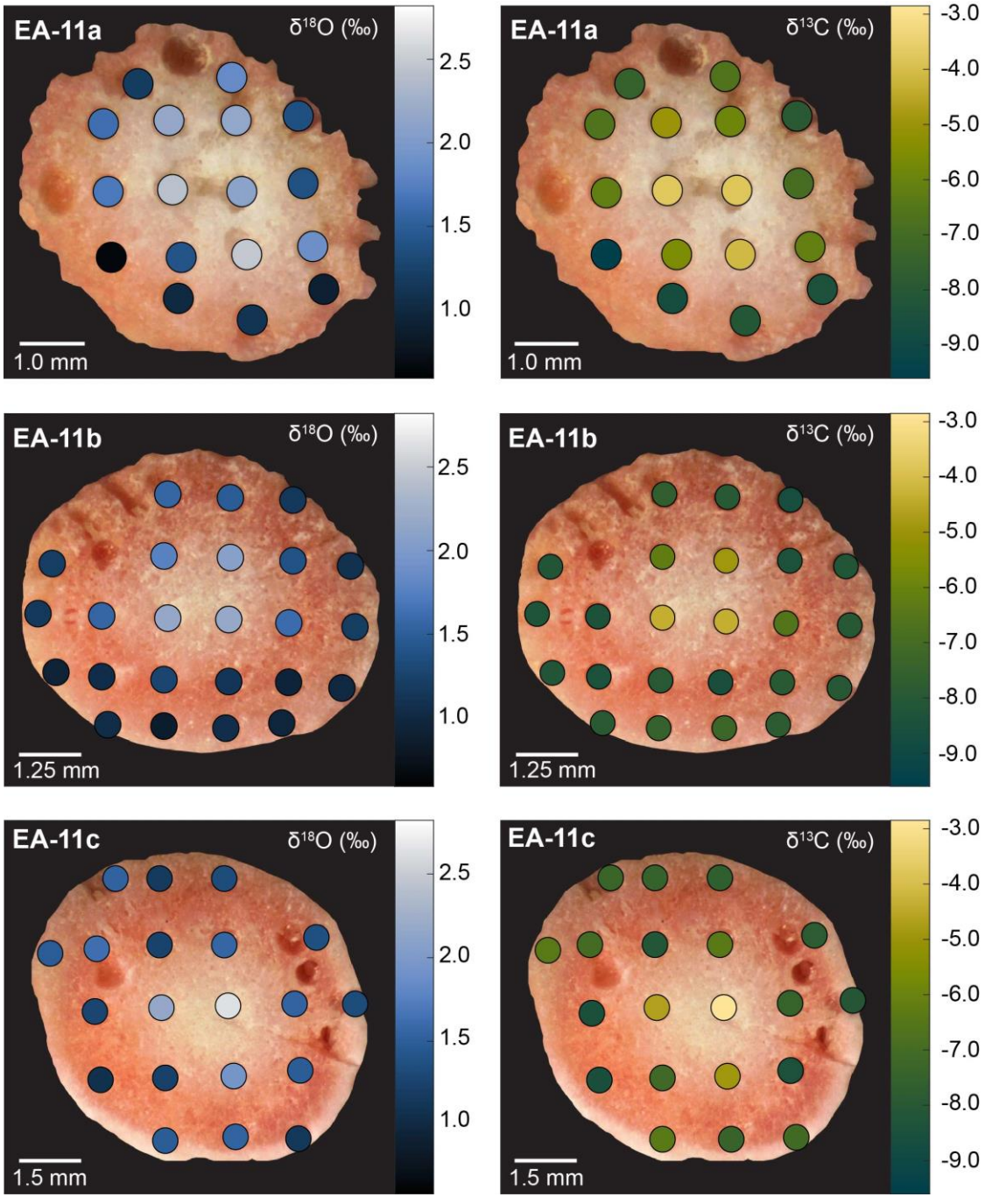

Figure 3: Stable isotope ratio maps for specimens EA-11 and EA-12 slices. Each row represents a pair of measurements: left column being $\delta^{18}O$ values and right column $\delta^{13}C$ values. $\delta^{18}O$ and $\delta^{13}C$ values are marked by colored circles on each map with corresponding adjacent color bar. Values are expressed in per mil (‰) relative to PDB, and analytical uncertainty (1σ) during this study was ±0.064 ‰ $\delta^{18}O$ and ±0.083 ‰ $\delta^{13}C$. All slices exhibit the same feature of the largest isotopic values toward the inner white section, which is not always the geometric center of the slice.

https://doi.org/10.5194/bg-2022-180
Preprint. Discussion started: 4 October 2022

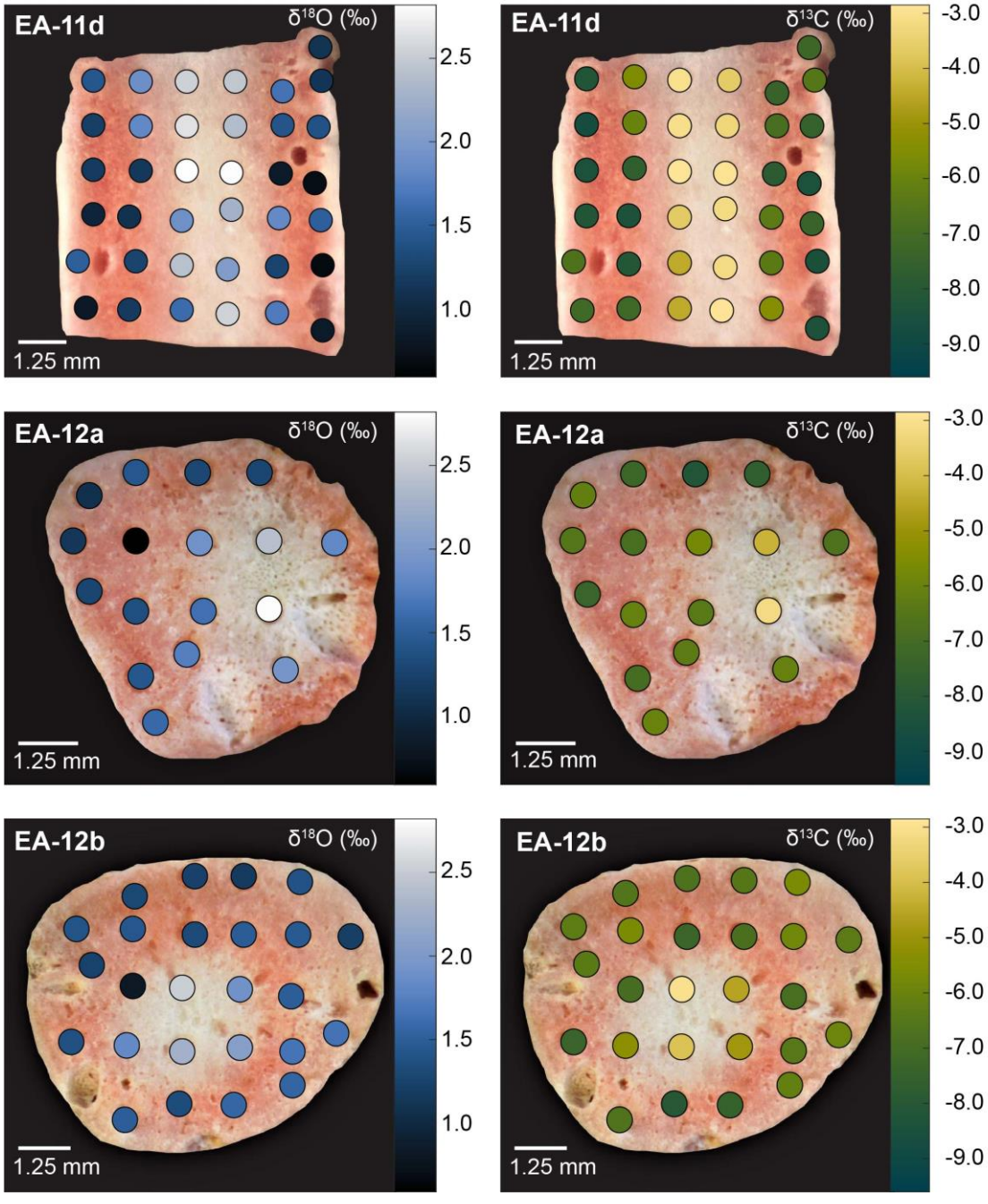

Figure 3 continued.

https://doi.org/10.5194/bg-2022-180
Preprint. Discussion started: 4 October 2022

biocalcification process that does not depend on annual (or regularly paced) precipitation of carbonate skeleton. The larger range of values observed over EA-11d is not as surprising as it could be due to the sampling scheme for this slice covering a larger vertical distance of coral than the others (i.e., transecting more time).

For specimen EA-12, $\delta^{18}O$ values range from 0.60‰ to 2.81‰, and $\delta^{13}C$ values range from -8.18 ‰ to -2.99 ‰, similar to those exhibited by EA-11. Minimum $\delta^{18}O$ and $\delta^{13}C$ values for EA-12 were both exhibited by slice EA-12a, nearest the tip. The maximum values, however, are split between slices (maximum $\delta^{18}O$ at EA-12a and maximum $\delta^{13}C$ at EA-12b). The $\delta^{18}O$ values recorded by EA-12a range from 0.60 ‰ to 2.81 ‰ and $\delta^{13}C$ values span -8.18 ‰ to -3.19 ‰. For EA-12b, the $\delta^{18}O$ values span from 0.82 ‰ to 2.53 ‰ and $\delta^{13}C$ values span -8.02 ‰ to -2.99 ‰. The range of $\delta^{18}O$ and $\delta^{13}C$ values over each of the EA-12 slices are on the order of ~2 ‰ and ~5 ‰, similar to EA-11. This suggests that the magnitude of vital effects could be consistent among this stylasterid taxon.

4 Discussion

4.1 Isotopic disequilibrium

Vital effects are observed over each coral slice, as evidenced by both the disparity between measured isotopic values and calculated equilibrium, and the range of measured values (Figs. 3 and 4). Carbonate isotopic equilibrium values were calculated for both calcite and aragonite as stylasterids have exhibited mixed mineralogy (Cairns and Macintyre, 1992). Calcite and aragonite $\delta^{13}C$ equilibrium values were calculated using equations from Romanek et al. (1992), and calcite and aragonite $\delta^{18}O$ equilibrium values were calculated using equations from Grossman and Ku (1986) and O'Neil et al. (1969), respectively. The seawater isotopic values and temperature were determined using the average composition of the 500–1700 m depth range (similar to the coral collection depths) at stations nearest the coral dredge sites reported by the Geochemical Ocean Sections Program (GEOSECS; Fig. 1; (Schmidt et al., 1999; Schlitzer, 2022). The resulting calcite equilibrium is 3.55 ± 0.08 ‰ for $\delta^{18}O$ and 1.31 ± 0.30 ‰ for $\delta^{13}C$, and aragonite equilibrium is 4.44 ± 0.07 ‰ for $\delta^{18}O$

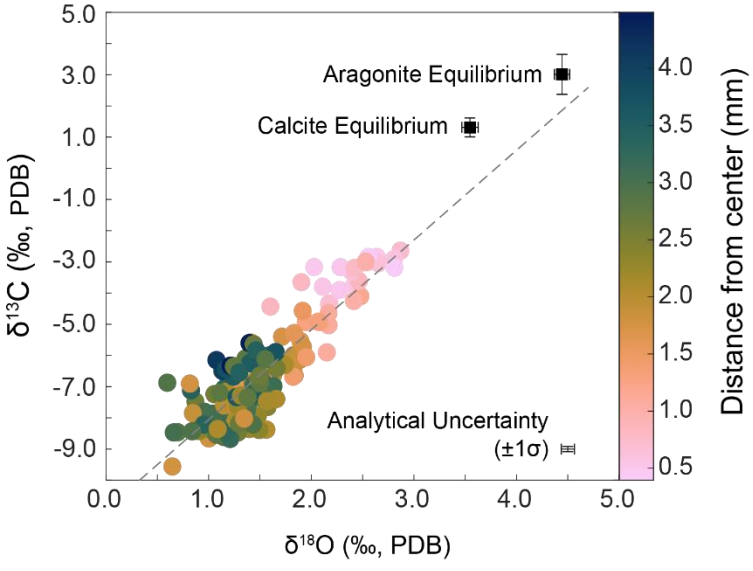

Figure 4: All stylasterid oxygen and carbon isotopes reported relative to PDB. Color represents the distance from the coral center and corresponds to the color bar at the right. Calculated equilibrium values are also shown as the black squares (see text for further explanation). The dashed gray line represents the line of best fit for the measured values ($\delta^{13}C$ = 2.88 (±0.14) * $\delta^{18}O$-10.94 (±0.22)). The measured values closest to equilibria are those toward the center of each coral disc, as noted by the darker colors.

https://doi.org/10.5194/bg-2022-180
Preprint. Discussion started: 4 October 2022

Biogeosciences Discussions Open Access EGU

and 3.01 ± 0.64 ‰ for $\delta^{13}C$ (Fig. 4; Table S2 in the Supplement). The minimum depletion by 0.68 ‰ and 3.95 ‰ from oxygen and carbon isotope equilibrium, respectively, represent calcification largely influenced by vital effects. Furthermore, if the $\delta^{18}O$ variability is assumed to represent an environmental signal recorded in the stylasterid carbonate at equilibrium, the magnitude of those changes would be unrealistic. Using the stylasterid temperature calibration from Samperiz et al. (2020), we calculate the temperature change to be up to ~7° C across each coral slice and ~10° C along the vertical section of EA-11d. Such temperature changes are too large for the Southern Ocean over the lifespan of a single coral specimen. Therefore, isotopic variability observed here supports calcification out of equilibrium with ambient sea water and a significant influence by vital effects.

We observe a strong linear correlation between $\delta^{18}O$ and $\delta^{13}C$ values, a common feature among biological marine calcifiers, and expected here. The compilation of samples in this study result in a linear trend with a slope of 2.88 ± 0.14 ($\Delta\delta^{13}C/\Delta\delta^{18}O$; R^2=0.76) or 0.26 ±0.01 ($\Delta\delta^{18}O/\Delta\delta^{13}C$; R^2=0.76) that passes near the calculated equilibrium values (Fig. 4). Although extreme variability has been observed among the slopes of deep-sea coral isotope records (Emiliani et al., 1978; Smith et al., 2000, 2002; Adkins et al., 2003; Wisshak et al., 2009; Hill et al., 2011; Samperiz et al., 2020), the slope here falls within the range of reported values for deep-sea stylasterid corals (Samperiz et al., 2020). A notable difference from previous work is the minimum offset between calculated equilibrium and measured $\delta^{18}O$ and $\delta^{13}C$ of these specimens (Figs. 4 and 5). As mentioned before, the minimum offset from equilibrium is 0.6 8‰ for $\delta^{18}O$ and 3.95 ‰ for $\delta^{13}C$, yet the Samperiz et al. (2020) compilation

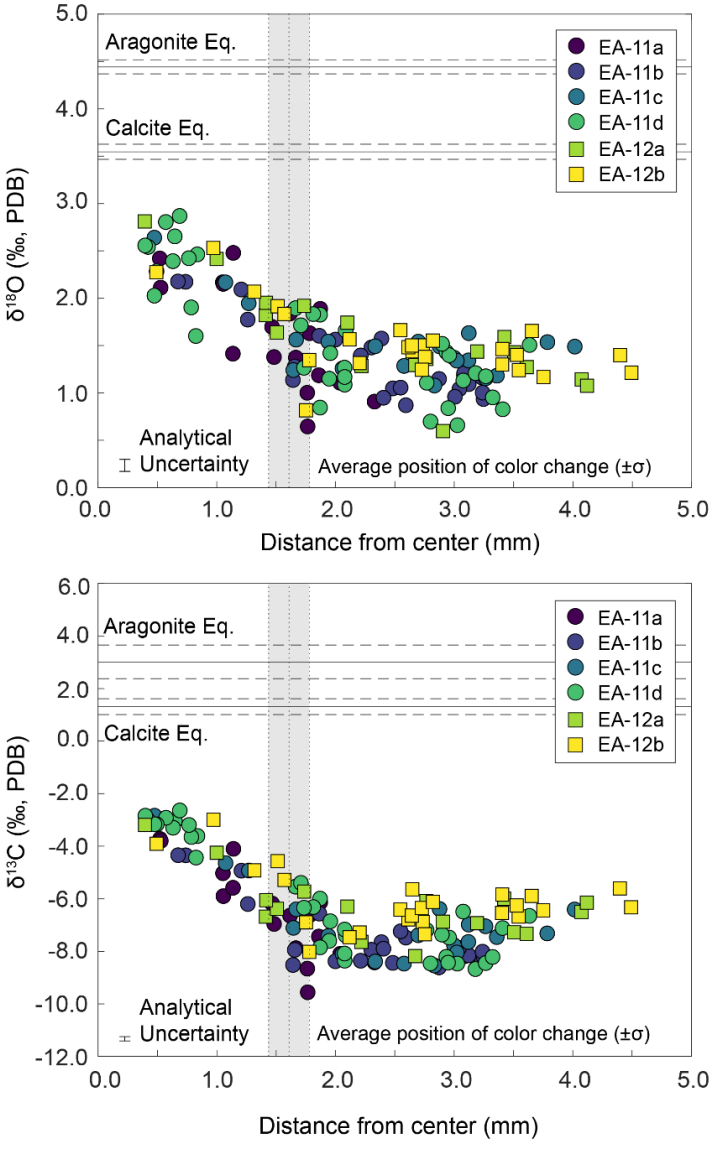

Figure 5: Oxygen (top) and carbon (bottom) stable isotope ratios by distance from the center of the coral. The values are plotted by slice from each specimen as noted by the circles (EA-11) and squares (EA-12). The horizontal lines denote calculated aragonite and calcite equilibrium values with corresponding uncertainty in dashed lines (±1σ). Vertical gray bars denote the average radius of the white coral center, the width of the bar denoting ±1σ. Note that there is no observable trend concerning coral slices (i.e., by distance from the coral tip), only the increase in isotopic values toward the white, center region of the corals.

https://doi.org/10.5194/bg-2022-180
Preprint. Discussion started: 4 October 2022

is characterized by a much smaller minimum offset of approximately 0.025 ‰ for $\delta^{18}O$ and 1‰ for $\delta^{13}C$. The magnitude of the offset in this study could be due in part to inaccuracies in the calculated equilibrium values; this includes both the oceanographic data not being representative of the coral growth environment and mineralogical endmember calculations. Carbonate equilibrium calculations were based on equations for aragonite–seawater fractionation (Grossman and Ku, 1986; Romanek et al., 1992) and calcite–seawater fractionation (O'Neil et al., 1969; Romanek et al., 1992), however, if the coral mineralogy includes a mixture, the values could be further offset. We have evidence for mixed mineralogy within these specimens, but additional work needs to be done to approximate the mineralogy over the sampled discs.

4.2 Isotopic trends and calcification models

In order to grow dendritically, the most intuitive growth model for corals such as our stylasterids holds that the center of each branch extends axially faster than each branch thickens radially. Thus, the kinetic effects would be most apparent in the center of each coral slice and lessen towards the outer edges, resulting in $\delta^{18}O$ and $\delta^{13}C$ values that would therefore approach equilibrium toward the edges of each isotope map. Many marine calcifying organisms (e.g., mollusks and corals) follow the Von Bertalanaffy growth model wherein their calcification rate ontogenetically decreases, and we posited that this model also applied to the horizontal extension of stylasterids as they prioritize vertical growth (Ralph and Maxwell, 1977; Emiliani et al., 1978; Berkman, 1990; Philipp et al., 2005; Román-González et al., 2017). Such a coral growth model is supported by observations from Fallon et al. (2014) wherein a cold water scleractinian coral demonstrated growth similar to stacking cones with a fast growing tip. This structure is also supported by isotopic records of other stylasterids and bamboo corals which were all characterized by low isotopic values at the regions of most rapid growth (Wisshak et al., 2009; Samperiz et al., 2020; Hill et al., 2011).

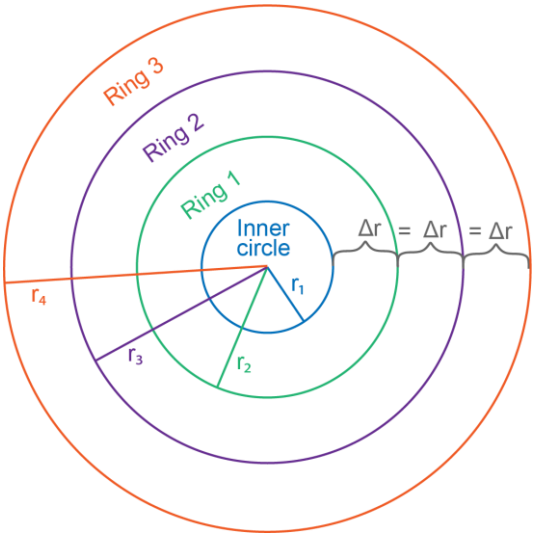

Figure 6: Coral slice schematic used for calcification models. In this simplified model, growth begins with the inner circle of radius r_1. Each growth increment is noted by a new ring, Ring n, with a radius, r_{n+1}. In this case, the change in radius between each ring, Δr, is equal representing the constant radial extension model. The Δr becomes larger or smaller with each ring for the increasing and degreasing growth scenarios, respectively.

To better understand our resulting trends, we created models that reflect simplified calcification scenarios of constant, decreasing, and increasing radial extension with time. The model calculations were based on an idealized coral slice of n rings with radii, r_{n+1}, an initial growth inner circle of radius, r_1, and the extension rate represented by the change in radius, Δr, between each ring (Fig. 6). We set each model to run for 100 years and examined the rate of change of coral area as a proxy for calcification rate in each scenario. Because the radial extension of *Errina* corals is largely unknown, we employed a range of horizontal growth rates reported for live-collected bamboo corals living at a depth

https://doi.org/10.5194/bg-2022-180
Preprint. Discussion started: 4 October 2022

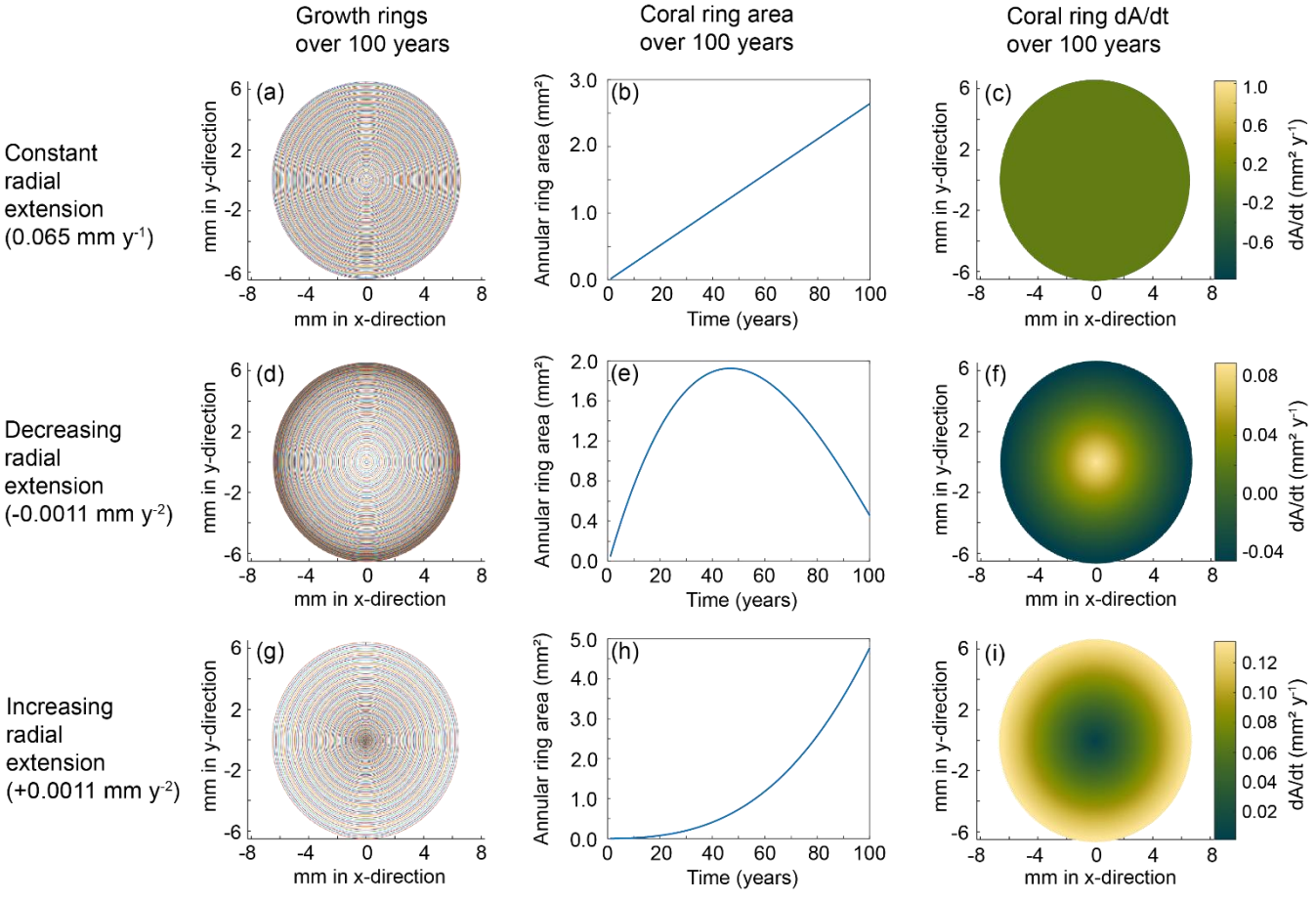

Figure 7: Coral calcification models for each scenario. The top row (a–c) depicts results from the constant radial extension model, the middle row (d–f) is the decreasing radial extension, and the bottom row (g–i) is the increasing radial extension model. The left column depicts the growth rings for each model after a run of 100 years. The middle column shows the change in area with each year of calcification. The right column shows the rate of change in coral area for each model. The corresponding color bars represent the magnitude of change.

To determine which growth scenario likely represents our stable isotope maps, we defined changes in calcification rate as the two-dimensional changes in coral area with time. We then compared the resulting models to the changes in stable isotope

https://doi.org/10.5194/bg-2022-180
Preprint. Discussion started: 4 October 2022

values across each coral slice (assuming no change in the ambient seawater values during the time of precipitation). In the case of the constant radial extension, the growth rings are evenly spaced, leading to a steady increase of horizontal area between the rings with time (Fig. 7a and b). Constant radial extension refers to constant change in area with time (Fig. 7c). Such a growth model would result in stable isotope values to either be constant across the surface of the coral or record any changes that reflect seawater variability. Decreasing radial extension with time relates to decreasing area with time (Fig. 7d–f). We hypothesized decreasing radial extension to be the most likely calcification pattern as the available literature supports slowing growth with time. With a decreasing radial extension, the growth bands become closer with time, causing the area to increase then decrease over the modeled 100 year span (Fig. 7d and e). Therefore, the rate of change of area decreases toward the outer edges of the coral surface (Fig. 7f). Because faster calcification results in stronger vital effects, the center of the coral would exhibit isotope values furthest from equilibrium. That is the opposite of what we observed. The increasing radial extension scenario led to growth bands increasing distance from each other, resulting in an exponential increase in area (Fig. 7g and h). The resulting calcification scheme (i.e., rate of change in area) would lead to stronger vital effects toward the outer edges of the coral surface and isotopic values closer to equilibrium in the center (Fig. 7i). This is what we observed.

The unique pattern of the highest isotopic values in the center of the coral with lower values toward the mid and outer edge rejects our hypothesis for calcification and is contradicted by previously published isotope records and growth models. The stable isotope maps instead support rapid calcification toward the outer region and slow calcification in the center. Such a model, however, is not supported by previously mentioned growth habits of marine carbonates and would not result in dendritic corals. Several studies involving scleractinian corals and octocorals (class Anthozoa whereas stylasterids are class Hydrozoa) have converged on similar two-stage calcification patterns. Using X-ray micro-computed tomography, Urushihara et al. (2016) were able to determine that the cold water octocoral, *Corallium konojoi* (~290 m water depth), calcifies by two processes: formation of sclerites (small aggregates of carbonate within the coenenchyme tissue surrounding polyps) and a combined sclerite/biomineralization process at the apical region where skeletogenic epithelium secretes carbonate. A similar growth strategy was observed using incubated octocorals, *Corallium rubrum* (~20 m water depth), and measuring uptake of isotopic tracers (Allemand and Benazet-Tambutte, 1996). The authors found that the red coral forms its axial skeleton via biomineralization from the skeletogenic epithelium, which contributes to its horizontal extension. At the apical region, spicules fuse with the skeleton for vertical extension (Allemand and Benazet-Tambutte, 1996). Additional isotopic labeling experiments involving the zooxanthellate scleractinian, *Porites porites* (~50 m water depth), identified "hot spots" of calcification wherein biomineralization was not uniform across the growing surface of the coral (Houlbrèque et al., 2009). The authors attributed the heterogeneous calcification to an uneven distribution of extracellular calcifying fluid within the coral (Houlbrèque et al., 2009). Calcification strategies that invoke uneven, or two-step biomineralization could account for the regional distribution of vital effects observed in our coral isotope maps.

https://doi.org/10.5194/bg-2022-180
Preprint. Discussion started: 4 October 2022

A growth model of shallow water staghorn coral (*Acropora cervicornis*) over daily to yearly timescales best reconciles our data (Gladfelter 1982, 1983, 1984). . The Gladfelter model includes two main phases: rapid extension by randomly oriented crystals that develop the main skeletal framework, followed by infilling and strengthening of the skeleton along the entire growth axis (Gladfelter, 1982). Gladfelter (1983) observed that the initial framework growth was largely around the mid and outer regions of the corallite and the infilling occurred later in the center. We posit that this model accurately describes the stylasterid coral growth here as the lower isotopic values toward the outer edge signify enhanced kinetic fractionation from rapid growth to develop an initial framework. As the center region of the coral thickens and strengthens, kinetic fractionation is reduced resulting in higher isotopic values, closer to equilibrium. Additionally, Gladfelter (1982) noted increasing mineralization from the tip of the staghorn coral to about 30 mm, after which the mineralization was roughly constant. This description suits our isotopic record in that the overall lightest value was near the growth tip and the heaviest value near the base, reflecting the higher proportion of slowly precipitated skeleton lower down on the coral. Our unique isotope records support the Gladfelter growth model, and greatly improve our understanding of the formation of a valuable paleoceanographic archive.

4.3 Considerations for paleoceanographic reconstructions

The definitive trend of increasing isotopic values toward the inner, white section of the coral support that this is the ideal region of the coral from which to sample for paleotemperature reconstructions. Because the higher values are located nearest the white section of the coral and not the geometric center, we converted the images of each slice to grayscale (Fig. 8). This allowed for us to find the whitest pixels and quantitatively determine the most ideal location for sampling. With the exception of the light outer edges, the sample holes that were at least 75 % surrounded by the whitest pixels were selected for temperature reconstructions (Fig. 8). These $\delta^{18}O$ values were averaged for each coral slice and were used with the stylasterid temperature calibration from Samperiz et al. (2020). Additionally, the $\delta^{18}O$ average for each entire slice was calculated to determine a "bulk" value that would represent a common sampling method of drilling across the growth axis. The bulk $\delta^{18}O$ values were also calibrated to temperature and the results are illustrated in Fig. 9 (Table S3 in the Supplement). Note that for slice EA-11d that consists of a vertical face rather than horizontal, $\delta^{18}O$ values were only combined for the same distance from the coral tip.

Although both the "central" and "bulk" temperature records are higher than current ocean temperatures of a similar depth, the center values are significantly different from bulk measurements, and are closer to the true environmental signal (Fig. 9). We compared the center and bulk temperature records using the Student's t-Test to determine whether the difference between the means are significant or occurred by chance (from variability). We used a paired t-Test to compare center and bulk temperatures from the same distance from the tip where available. With a p-value of 6.61×10^{-6}, the difference between center and bulk temperatures is very unlikely to have occurred by chance (Table S4 in the Supplement). This analysis, however, assumes no environmental change over the lifespan of the corals. To account for possible seawater changes and more accurately reflect the samples that would be targeted for temperature reconstructions, we also tested individual temperatures across each

https://doi.org/10.5194/bg-2022-180
Preprint. Discussion started: 4 October 2022

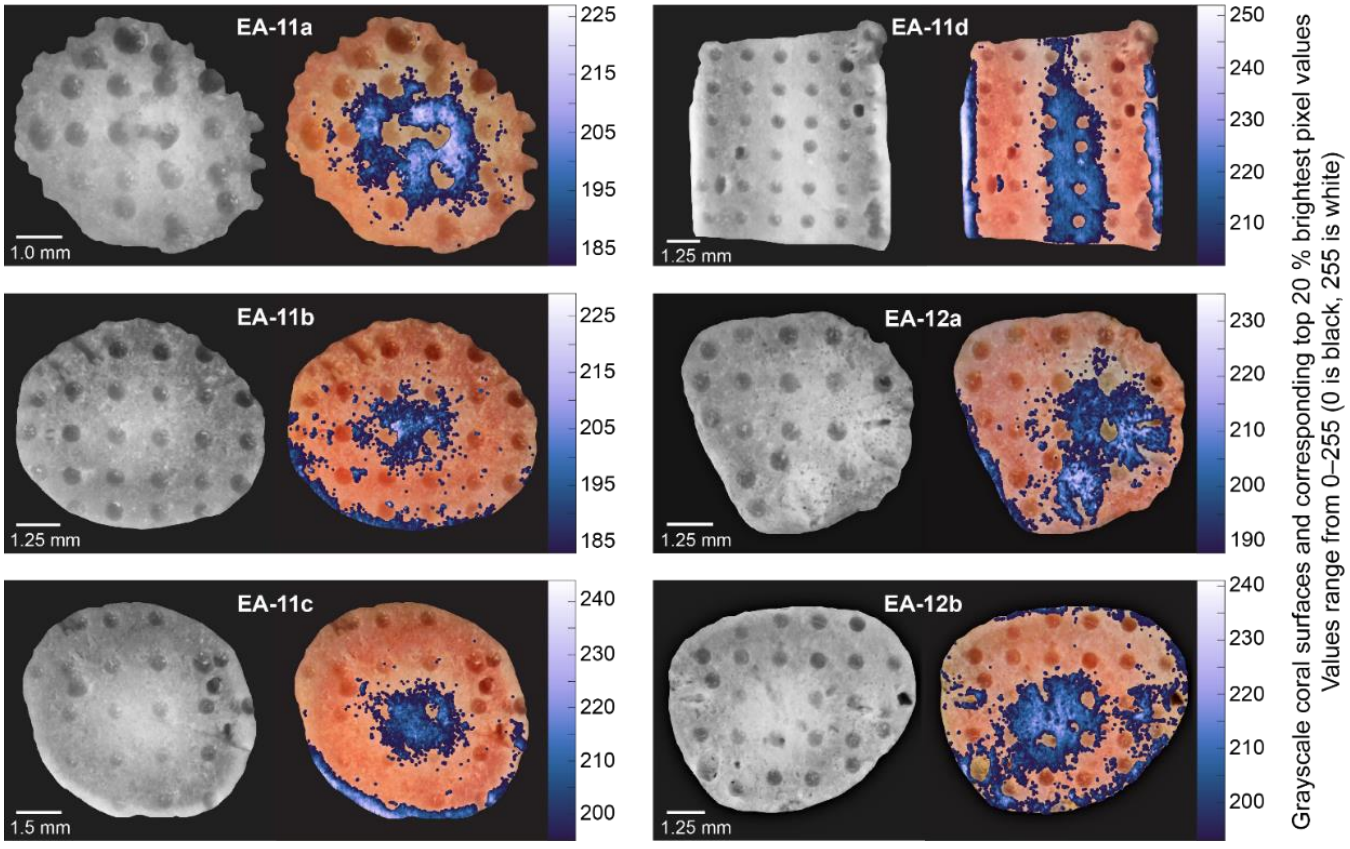

Figure 8: Compilation of grayscale images and corresponding brightest pixels (highest 20 %) over each coral slice. The colors correspond to the grayscale pixel value (higher on the scale bar denotes a whiter pixel). The sample holes surrounded by at least ~75 % of bright pixels were used to calculate representative $\delta^{18}O$ values for each slice for temperature calibration (Table S3 in the Supplement).

slice (rather than the averages used in Fig. 9). The unpaired t-Test required at least two temperature values that were sampled from the white center and the pink outer regions for at least one degree of freedom. This was met by four coral slices, EA-11a, EA-11b, EA-11d (63.55 mm from the tip), and EA-12b; each test producing p-values less than 0.005 (Table S4 in the Supplement). These analyses show that we can conceive of no comparison within coral slices that show the same values between the center and bulk temperatures.

Figure 9 shows that detailed analysis of isotopic distributions through stylasterid skeletons does not quite achieve samples representative of isotope equilibrium; but closer approach is possible. If finer-scale samples were informed with computerized tomography (CT) scanning methods, we posit that our prescribed sampling scheme for these corals can yield robust paleotemperature records. Sampled as we have, with even distribution of samples over the surface of each disc as a goal, our reconstructed temperatures are higher than a likely environmental signal. However, we have demonstrated that the center white region of the coral is less affected by vital effects and less likely altered after initial deposition. Therefore, we recommend

https://doi.org/10.5194/bg-2022-180
Preprint. Discussion started: 4 October 2022

sampling of the white center using more spatially precise micro-milling methods to target even smaller regions, thus minimizing the impact of vital effects. We also note that in calculating uncertainty associated with temperature calibrations, our center temperature errors are likely underestimated as they rely largely on the analytical uncertainty. However, our calculation of temperatures from bulk data includes high spatial standard deviations; more precise sampling would yield more precise temperature estimates. Thus, a targeted milling approach would likely reflect a more accurate uncertainty estimate on the temperature as well. Additionally, CT scanning that reveals coral growth structures, such as Urushihara et al. (2016), would improve allow an even closer approach to accurate paleoceanographic reconstructions. Such combined methods would allow for extremely targeted sampling considering both the growth structure and biomineralization methods to inform sampling efforts to allow closer approach to equilibrium and better accuracy of paleotemperature reconstructions using *Errina* corals.

5 Conclusions

The results presented here can assuage a considerable hesitation for the paleoceanographic community surrounding the influence of vital effects on stylasterid coral paleo-archives. We have demonstrated that deep-sea stylasterid corals exhibit significant vital effects that obscure the environmental signal; however, we are also able to provide maps that guide future coral sampling efforts. Lacking any visible banding structure, the *Errina* specimens in this study benefitted from a gridded sampling scheme to determine the location of minimum influence from vital effects. Our skeletal $\delta^{18}O$ and $\delta^{13}C$ values exhibit an increasing trend toward seawater equilibrium near the

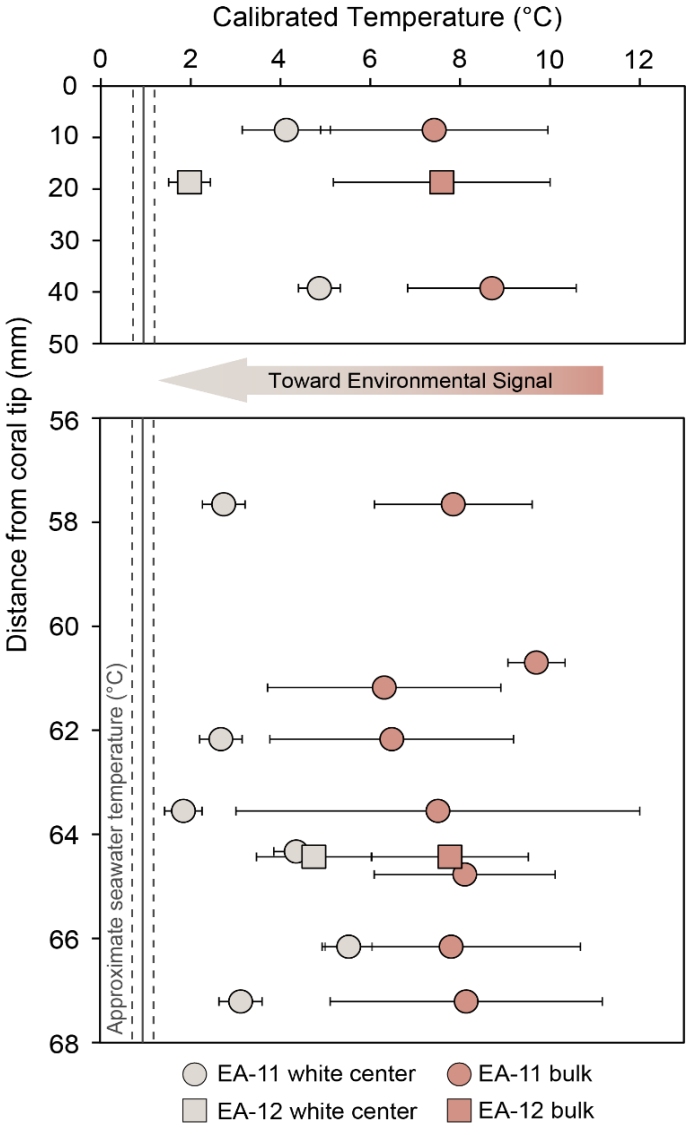

Figure 9: Temperature calibration using the equation from Samperiz et al. (2020). Light colored points denote temperatures using the $\delta^{18}O$ values from the white centers of each slice, whereas the darker, peach color denote a "bulk" measurement. The bulk is calculated using the average $\delta^{18}O$ of the entire slice, similar to a value that would be measured from a sample collected via drilling into the side of a coral specimen. Error bars are based on standard deviation of three or more averaged samples. The error bars for less than three samples are based on the analytical error propagation (Table S3 in the Supplement).

https://doi.org/10.5194/bg-2022-180
Preprint. Discussion started: 4 October 2022

center of the coral. This result contradicts growth structures hypothesized in the current body of literature based on observed stable isotopic trends (Wisshak et al., 2009; Samperiz et al., 2020; Hill et al., 2011), but supports a two-stage growth model that describes a "hasty" initial lattice framework construction, followed by slower infilling to strengthen, and support the coral colony (Gladfelter, 1982, 1983). The samples from the center white region of the corals produced temperature records significantly different than a bulk approach and were closest to nearby ocean temperatures. Thus, we recommend sampling along the center, white region where the infilling has allowed for calcification closest to seawater equilibrium and an environmental isotopic signal. Further, we suggest initial CT scanning of corals to determine any hidden growth features, and micro milling sampling techniques to target the location of the most accurate record. Combined with a new stylasterid temperature calibration (Samperiz et al., 2020), we posit that accurate paleotemperature records can be reconstructed from deep-sea *Errina* corals.

Data availability

All data are available in the supplement.

Author contributions

Both authors contributed to the conceptualization of the work. TMK developed sampling methods under the supervision of BER. Both authors contributed to formal analysis. TMK wrote the manuscript draft, with significant input from BER. Both authors approved the final version of the manuscript.

Competing interests

The authors declare that they have no conflict of interest.

Acknowledgements

We thank the captain, crew, and scientific staff of the RV *Nathaniel B. Palmer* during the US Antarctic Program expedition NBP07-01 to the Ross Sea, Antarctica for their efforts in coral collection. We also thank Dr. Ernst Peebles for the use of laboratory space during coral sampling, and Drs. Jennifer Granneman and David Jones for guidance on both slicing the corals and initial setup of the MircoMill. During this project, TMK was funded through the Genshaft Family Dissertation Fellowship awarded by the University of South Florida as well as three endowed fellowships from the College of Marine Science: Carl Riggs Endowed Fellowship, George Lorton Fellowship in Marine Science, and the Abby Sallenger Memorial Award.

https://doi.org/10.5194/bg-2022-180
Preprint. Discussion started: 4 October 2022

References

Adkins, J. F., Cheng, H., Boyle, E. A., Druffel, E. R. M., and Edwards, R. L.: Deep-Sea Coral Evidence for Rapid Change in Ventilation of the Deep North Atlantic 15,400 Years Ago, Science, 280, 725–728, https://doi.org/10.1126/science.280.5364.725, 1998.

Adkins, J. F., Boyle, E. A., Curry, W. B., and Lutringer, A.: Stable isotopes in deep-sea corals and a new mechanism for "vital effects," Geochim. Cosmochim. Ac., 67, 1129–1143, https://doi.org/10.1016/S0016-7037(02)01203-6, 2003.

Allemand, D. and Benazet-Tambutte, S.: Dynamics of calcification in the mediterranean red coral, Corallium rubrum (Linnaeus) (Cnidaria, Octocorallia), J. Exp. Zool., 276, 270–278, https://doi.org/10.1002/(SICI)1097-010X(19961101)276:4<270::AID-JEZ4>3.0.CO;2-L, 1996.

Andrews, A. H., Cordes, E. E., Mahoney, M. M., Munk, K., Coale, K. H., Cailliet, G. M., and Heifetz, J.: Age, growth and radiometric age validation of a deep-sea, habitat-forming gorgonian (Primnoa resedaeformis) from the Gulf of Alaska, Hydrobiologia, 471, 101–110, https://doi.org/10.1023/A:1016501320206, 2002.

Arndt, J. E., Schenke, H. W., Jakobsson, M., Nitsche, F. O., Buys, G., Goleby, B., Rebesco, M., Bohoyo, F., Hong, J., Black, J., Greku, R., Udintsev, G., Barrios, F., Reynoso-Peralta, W., Taisei, M., and Wigley, R.: The International Bathymetric Chart of the Southern Ocean (IBCSO) Version 1.0-A new bathymetric compilation covering circum-Antarctic waters: IBCSO VERSION 1.0, Geophys. Res. Lett., 40, 3111–3117, https://doi.org/10.1002/grl.50413, 2013.

Berkman, P. A.: The population biology of the Atarctic scallop, Adamussium colbecki (Smith 1902) at New Harbor, Ross Sea, in: Antarctic Ecosystems, edited by: Kerry, K.R. and Hempel, G., Springer, Berlin, Heidelberg, Germany, 281–288, https://doi.org/10.1007/978-3-642-84074-6_32, 1990.

Burke, A. and Robinson, L. F.: The Southern Ocean's Role in Carbon Exchange During the Last Deglaciation, Science, 335, 557–561, https://doi.org/10.1126/science.1208163, 2012.

Cairns, S. D.: A generic revision of the Stylasterina (Coelenterata: Hydrozoa). Part 1, Description of the genera, B. Mar. Sci., 33, 427-508, 1983a.

Cairns, S. D.: Antarctic and Subantarctic Stylasterina (Coelenterata: Hydrozoa), in: Biology of the Antarctic Seas XIII, vol. 38, edited by: Kornicker, S., American Geophysical Union, Washington, D. C., USA, 61–164, 1983b.

Cairns, S. D.: A generic revision of the Stylasteridae (Coelenterata: Hydrozoa). (Coelenterata: Hydrozoa). Part 3, Keys to the genera, B. Mar. Sci., 49, 538-545, 1991.

Cairns, S. D.: Worldwide distribution of the Stylasteridae (Cnidaria: Hydrozoa), Sci. Mar., 56, 125–130, 1992.

Cairns, S. D. and Macintyre, I. G.: Phylogenetic Implications of Calcium Carbonate Mineralogy in the Stylasteridae (Cnidaria: Hydrozoa), PALAIOS, 7, 96-107, https://doi.org/10.2307/3514799, 1992.

Chen, S., Gagnon, A. C., and Adkins, J. F.: Carbonic anhydrase, coral calcification and a new model of stable isotope vital effects, Geochim. Cosmochim. Ac., 236, 179–197, https://doi.org/10.1016/j.gca.2018.02.032, 2018.

Chen, T., Robinson, L. F., Burke, A., Claxton, L., Hain, M. P., Li, T., Rae, J. W. B., Stewart, J., Knowles, T. D. J., Fornari, D. J., and Harpp, K. S.: Persistently well-ventilated intermediate-depth ocean through the last deglaciation, Nat. Geosci., https://doi.org/10.1038/s41561-020-0638-6, 2020.

https://doi.org/10.5194/bg-2022-180
Preprint. Discussion started: 4 October 2022

Druffel, E. R. M.: Geochemistry of corals: Proxies of past ocean chemistry, ocean circulation, and climate, P. Natl. Acad. Sci., 94, 8354–8361, https://doi.org/10.1073/pnas.94.16.8354, 1997.

Druffel, E. R. M., King, L. L., Belastock, R. A., and Buesseler, K. O.: Growth rate of a deep-sea coral using 210Pb and other isotopes, Geochim. Cosmochim. Ac., 54, 1493–1499, https://doi.org/10.1016/0016-7037(90)90174-J, 1990.

Emiliani, C.: Pleistocene temperatures, J. Geol., 63, 538–578, https://doi.org/10.1086/626295, 1955.

Emiliani, C., Hudson, J. H., Shinn, E. A., and George, R. Y.: Oxygen and carbon isotopic growth record in a reef coral from the Florida Keys and a deep-sea coral from Blake Plateau, Science, 202, 627–629, https://doi.org/10.1126/science.202.4368.627, 1978.

Epstein, S., Buchsbaum, R., Lowenstam, H., and Urey, H. C.: Revised carbonate-water isotopic temperature scale, Bull. Geol. Soc. Am., 64, 1315–1326, https://doi.org/10.1130/0016-7606(1953)64[1315:RCITS]2.0.CO;2, 1953.

Fallon, S. J., Thresher, R. E., and Adkins, J.: Age and growth of the cold-water scleractinian Solenosmilia variabilis and its reef on SW Pacific seamounts, Coral Reefs, 33, 31–38, https://doi.org/10.1007/s00338-013-1097-y, 2014.

Gerrish, L., Fretwell, P., & Cooper, P., High resolution vector polylines of the Antarctic coastline (7.5), UK Polar Data Centre, Natural Environment Research Council, UK Research & Innovation [Basemap] https://doi.org/10.5285/bc71347d-298a-4df3-88b0-cb9a908db166, 2022.

Gladfelter, E. H.: Skeletal development in Acropora cervicornis: I. Patterns of calcium carbonate accretion in the axial corallite, Coral Reefs, 1, 45–51, https://doi.org/10.1007/BF00286539, 1982.

Gladfelter, E. H.: Skeletal Development in Acropora cervicornis: II. Diel patterns of calcium carbonate accretion, Coral Reefs, 2, 91–100, https://doi.org/10.1007/BF02395279, 1983.

Gladfelter, E. H.: Skeletal Development in Acropora cervicornis: III. A comparison of monthly rates of linear extension and calcium carbonate accretion measured over a year, Coral Reefs, 3, 51–57, https://doi.org/10.1007/BF00306140, 1984.

Gordon, A. L., Orsi, A. H., Muench, R., Huber, B. A., Zambianchi, E., and Visbeck, M.: Western Ross Sea continental slope gravity currents, Deep-Sea Res. Pt. II, 56, 796–817, https://doi.org/10.1016/j.dsr2.2008.10.037, 2009.

Griffin, S. and Druffel, E. R. M.: Sources of Carbon to Deep-Sea Corals, Radiocarbon, 31, 533–543, https://doi.org/10.1017/S0033822200012121, 1989.

Grossman, E. L. and Ku, T.-L.: Oxygen and carbon isotope fractionation in biogenic aragonite: temperature effects, Chem. Geol. (Isotope Geoscience Section), 59, 59-74, https://doi.org/10.1016/0168-9622(86)90057-6, 1986.

Heikoop, J. M., Dunn, J. J., Risk, M. J., Schwarcz, H. P., McConnaughey, T. A., and Sandeman, I. M.: Separation of kinetic and metabolic isotope effects in carbon-13 records preserved in reef coral skeletons, Geochim. Cosmochim. Ac., 64, 975–987, https://doi.org/10.1016/S0016-7037(99)00363-4, 2000.

Hill, T. M., Spero, H. J., Guilderson, T., LaVigne, M., Clague, D., Macalello, S., and Jang, N.: Temperature and vital effect controls on bamboo coral (*Isididae*) isotope geochemistry: A test of the "lines method", Geochem. Geophy. Geosy., 12, 14, https://doi.org/10.1029/2010GC003443, 2011.

Houlbrèque, F., Meibom, A., Cuif, J.-P., Stolarski, J., Marrocchi, Y., Ferrier-Pagès, C., Domart-Coulon, I., and Dunbar, R. B.: Strontium-86 labeling experiments show spatially heterogeneous skeletal formation in the scleractinian coral *Porites porites*, Geophys. Res. Lett., 36, L04604, https://doi.org/10.1029/2008GL036782, 2009.

Jacobs, S. S., Amos, A. F., and Bruchhausen, P. M.: Ross Sea oceanography and Antarctic Bottom Water formation, Deep-Sea Res. and Oceanographic Abstracts, 17, 935–962, https://doi.org/10.1016/0011-7471(70)90046-X, 1970.

Kurtz, D. D. and Bromwich, D. H.: A recurring, atmospherically forced polynya in Terra Nova Bay, in: Oceanology of the Antarctic Continental Shelf, vol. 43, edited by: Jacobs, S., American Geophysical Union, Washington, D. C., USA, 177–201, 1985.

Matsuoka, K., Skoglund, A., Roth, G., de Pomereu, J., Griffiths, H., Headland, R., Herried, B., Katsumata, K., Le Brocq, A., Licht, K., Morgan, F., Neff, P. D., Ritz, C., Scheinert, M., Tamura, T., Van de Putte, A., van den Broeke, M., von Deschwanden, A., Deschamps-Berger, C., Van Liefferinge, B., Tronstad, S., and Melvær, Y.: Quantarctica, an integrated mapping environment for Antarctica, the Southern Ocean, and sub-Antarctic islands, Environ. Modell. Softw., 140, 105015, https://doi.org/10.1016/j.envsoft.2021.105015, 2021.

McConnaughey, T.: 13C and 18O isotopic disequilibrium in biological carbonates: I. Patterns, Geochim. Cosmochim. Ac., 53, 151-162, https://doi.org/10.1016/0016-7037(89)90282-2, 1989a.

McConnaughey, T.: 13C and 18O isotopic disequilibrium in biological carbonates II. In vitro simulation of kinetic isotope effects, Geochim. Cosmochim. Ac., 53, 163–171, https://doi.org/10.1016/0016-7037(89)90283-4, 1989b.

McCrea, J. M.: On the Isotopic Chemistry of Carbonates and a Paleotemperature Scale, J. Chem. Phys., 18, 849–857, https://doi.org/10.1063/1.1747785, 1950.

Mikkelsen, N., Erlenkeuser, H., Killingley, J. S., and Berger, W. H.: Norwegian corals: radiocarbon and stable isotopes in Lophelia pertusa, Boreas, 11, 163–171, https://doi.org/10.1111/j.1502-3885.1982.tb00534.x, 2008.

Mouginot, J., B. Scheuchl, and E. Rignot. 2017. MEaSUREs Antarctic Boundaries for IPY 2007-2009 from Satellite Radar, Version 2 [Coastline and grounding line], Boulder, Colorado USA. NASA National Snow and Ice Data Center Distributed Active Archive Center, http://dx.doi.org/10.5067/AXE4121732AD, https://nsidc.org/data/nsidc-0709/versions/2, 2022.

O'Neil, J. R., Clayton, R. N., and Mayeda, T. K.: Oxygen Isotope Fractionation in Divalent Metal Carbonates, J. Chem. Phys., 51, 5547–5558, https://doi.org/10.1063/1.1671982, 1969.

Philipp, E., Brey, T., Pörtner, H.-O., and Abele, D.: Chronological and physiological ageing in a polar and a temperate mud clam, Mech. Ageing Dev., 126, 598–609, https://doi.org/10.1016/j.mad.2004.12.003, 2005.

Picco, P., Bergamasco, A., Demicheli, L., Manzella, G., Meloni, R., and Paschini, E.: Large-scale circulation features in the Central and Western Ross Sea (Antarctica), in: Ross Sea Ecology, Springer, Berlin, Heidelberg, Germany, 95–105, 2000.

Ralph, R. and Maxwell, J. G. H.: Growth of two Antarctic lamellibranchs: Adamussium colbecki and Laternula elliptica, Mar. Biol., 42, 171–175, https://doi.org/10.1007/BF00391569, 1977.

Risk, M. J., Heikoop, J. M., Snow, M. G., and Beukens, R.: Lifespans and growth patterns of two deep-sea corals: Primnoa resedaeformis and Desmophyllum cristagalli, Hydrobiologia, 471, 125–131, https://doi.org/10.1023/A:1016557405185, 2002.

Robinson, L. F. and van de Flierdt, T.: Southern Ocean evidence for reduced export of North Atlantic Deep Water during Heinrich event 1, Geology, 37, 195–198, https://doi.org/10.1130/G25363A.1, 2009.

Robinson, L. F., Adkins, J., Keigwin, L. D., Southon, J., Fernandez, D. P., Wang, S.-L., and Scheirer, D. S.: Radiocarbon variability in the Western North Atlantic during the Last Deglaciation, Science, 310, 1469–1473, https://doi.org/10.1126/science.1114832, 2005.

Robinson, L. F., Adkins, J. F., Frank, N., Gagnon, A. C., Prouty, N. G., Brendan Roark, E., and de Flierdt, T. van: The geochemistry of deep-sea coral skeletons: A review of vital effects and applications for palaeoceanography, Deep-Sea Res. Pt. II: Topical Studies in Oceanography, 99, 184–198, https://doi.org/10.1016/j.dsr2.2013.06.005, 2014.

Romanek, C. S., Grossman, E. L., and Morse, J. W.: Carbon isotopic fractionation in synthetic aragonite and calcite: Effects of temperature and precipitation rate, Geochim. Cosmochim. Ac., 56, 419–430, https://doi.org/10.1016/0016-7037(92)90142-6, 1992.

Román-González, A., Scourse, J. D., Butler, P. G., Reynolds, D. J., Richardson, C. A., Peck, L. S., Brey, T., and Hall, I. R.: Analysis of ontogenetic growth trends in two marine Antarctic bivalves Yoldia eightsi and Laternula elliptica: Implications for sclerochronology, Palaeogeography, Palaeoclimatology, Palaeoecology, 465, 300–306, https://doi.org/10.1016/j.palaeo.2016.05.004, 2017.

Samperiz, A., Robinson, L. F., Stewart, J. A., Strawson, I., Leng, M. J., Rosenheim, B. E., Ciscato, E. R., Hendry, K. R., and Santodomingo, N.: Stylasterid corals: A new paleotemperature archive, Earth Planet. Sc. Lett., 545, 116407, https://doi.org/10.1016/j.epsl.2020.116407, 2020.

Sandrini, S., Ait-Ameur, N., Rivaro, P., Massolo, S., Touratier, F., Tositti, L., and Goyet, C.: Anthropogenic carbon distribution in the Ross Sea, Antarctica, Antarct. Sci., 19, 395–407, https://doi.org/10.1017/S0954102007000405, 2007.

Schlitzer, R.: Ocean Data View [Seawater $\delta^{13}C$], https://odv.awi.de, 2021.

Schmidt, G. A., Bigg, G. R., and Rohling, E. J.: Global Seawater Oxygen-18 Database - v1.22 [Seawater $\delta^{18}O$], https://data.giss.nasa.gov/o18data/, 1999.

Shackleton, N.: Oxygen isotope analyses and Pleistocene temperatures re-assessed, Nature, 215, 15–17, https://doi.org/10.1038/215015a0, 1967.

Smith, J. E., Schwarcz, H. P., Risk, M. J., McConnaughey, T. A., and Keller, N.: Paleotemperatures from deep-sea corals: overcoming 'vital effects,' PALAIOS, 15, 25–32, 2000.

Smith, J. E., Schwarcz, H. P., and Risk, M. J.: Patterns of isotopic disequilibria in azooxanthellate coral skeletons, Hydrobiologia, 471, 111–115, https://doi.org/10.1023/A:1016553304276, 2002.

Swart, P. K.: Carbon and oxygen isotope fractionation in scleractinian corals: a review, Earth-Sci. Rev., 19, 51–80, https://doi.org/10.1016/0012-8252(83)90076-4, 1983.

Thresher, R., Tilbrook, B., Fallon, S., Wilson, N., and Adkins, J.: Effects of chronic low carbonate saturation levels on the distribution, growth and skeletal chemistry of deep-sea corals and other seamount megabenthos, Mar. Ecol. Prog. Ser., 442, 87–99, https://doi.org/10.3354/meps09400, 2011.

Urey, H. C.: The thermodynamic properties of isotopic substances, J. Chem. Soc. (Resumed), 562–581, https://doi.org/10.1039/jr9470000562, 1947.

Urushihara, Y., Hasegawa, H., and Iwasaki, N.: X-ray micro-CT observation of the apical skeleton of Japanese white coral Corallium konojoi, J. Exp. Mar. Biol. Ecol., 475, 124–128, https://doi.org/10.1016/j.jembe.2015.11.016, 2016.

https://doi.org/10.5194/bg-2022-180
Preprint. Discussion started: 4 October 2022

Weber, J. N.: Deep-sea ahermatypic scleractinian corals: isotopic composition of the skeleton, Deep-Sea Res. and Oceanographic Abstracts, 20, 901–909, https://doi.org/10.1016/0011-7471(73)90108-3, 1973.

Weber, J. N. and Woodhead, P. M. J.: Carbon and oxygen isotope fractionation in the skeletal carbonate of reef-building corals, Chem. Geol., 6, 93–117, https://doi.org/10.1016/0009-2541(70)90009-4, 1970.

Wisshak, M., López Correa, M., Zibrowius, H., Jakobsen, J., and Freiwald, A.: Skeletal reorganisation affects geochemical signals, exemplified in the stylasterid hydrocoral Errina dabneyi (Azores Archipelago), Mar. Ecol. Prog. Ser., 397, 197–208, https://doi.org/10.3354/meps08165, 2009.